

Final Draft
of the original manuscript:

Pangalos, M.; Bintig, W.; Schlingmann, B.; Feyerabend, F.; Witte, F.;
Begandt, D.; Heisterkamp, A.; Ngezahayo, A.:

**Action potentials in primary osteoblasts and in the MG-63
osteoblast-like cell line**

In: Journal of Bioenergetics and Biomembranes (2011) Springer

DOI: 10.1007/s10863-011-9354-7

Action potentials in primary osteoblasts and in the MG-63 osteoblast-like cell line

Maria Pangalos ¹, Willem Bintig ¹, Barbara Schlingmann ^{1, 2}, Frank Feyerabend ³, Frank Witte ⁵, Daniela Begandt ¹, Alexander Heisterkamp ⁴, Anaclet Ngezahayo ^{1, 2#}

¹ Institute of Biophysics, Leibniz University of Hannover, Herrenhäuserstr. 2, D-30419 Hannover, Germany

² Center for Systemic Neuroscience (ZSN), Hannover, Germany

³ Helmholtz-Zentrum Geesthacht, Institute of Materials Research, Department for Structural Research on Macromolecules, Max-Planck-Str. 1, 21502 Geesthacht, Germany

⁴ Laser Zentrum Hannover e.V., Hollerithallee 8, D-30419 Hannover, Germany

⁵ Implant-Immunology, CrossBIT - Center for Biocompatibility and Implant-Immunology, Hannover Medical School, Feodor-Lynen-Str. 31, D-30625 Hannover, Germany

Running title:

Ion channels in osteoblasts

Corresponding Author

Phone: +49-511 7624568

Fax: +49-511 7622606

E-mail: ngezahayo@biophysik.uni-hannover.de

Abstract

Whole-cell patch-clamp analysis revealed a resting membrane potential of -60 mV in primary osteoblasts and in the MG-63 osteoblast-like cells. Depolarisation-induced action potentials were characterised by duration of 60 ms, a minimal peak-to-peak distance of 180 ms, a threshold value of -20 mV and a repolarisation between the spikes to -45 mV. Expressed channels were characterised by application of voltage pulses between -150 mV and 90 mV in 10 mV steps, from a holding potential of -40 mV. Voltages below -60 mV induced an inward current. Depolarising voltages above -30 mV evoked two currents: (i) a fast activated and inactivated inward current at voltages between -30 and 30 mV, and (ii) a delayed-activated outward current that was induced by voltages above -30 mV. Electrophysiological and pharmacological parameters indicated that hyperpolarisation activated strongly rectifying K^+ (K_{ir}) channels, whereas depolarisation activated tetrodotoxin sensitive voltage gated Na^+ (Na_v) channels as well as delayed, slowly activated, non-inactivating, and tetraethylammonium sensitive voltage gated K^+ (K_v) channels. In addition, RT-PCR showed expression of $Na_v1.3$, $Na_v1.4$, $Na_v1.5$, $Na_v1.6$, $Na_v1.7$, and $K_{ir}2.1$, $K_{ir}2.3$, and $K_{ir}2.4$ as well as $K_v2.1$. We conclude that osteoblasts express channels that allow firing of action potentials.

Key words

Osteoblasts, MG-63 cells, Action potential, K_{ir} , K_v , Na_v , RT-PCR

Introduction

Repetitive action potentials, in response to a long lasting membrane depolarisation, are a characteristic of excitable cells, such as neurons, muscle cells or endocrine cells. The generation of action potentials is possible when cells express special types of voltage-gated channels (Bezanilla, 2007; Clay, 2005; Hodgkin and Huxley, 1952). These channels are closed when the membrane potential is maintained near the resting membrane potential and they open sequentially in response to membrane depolarisation above a defined threshold value. Voltage-gated Na^+ (Na_v) channels are the first channels that are opened by depolarisation. These channels allow an inward flow of Na^+ , which in turn, produces further depolarisation of the membrane. This effect causes more Na_v channels to open and produces an even greater electrical current. The process proceeds explosively, which results in a large increase in the membrane potential toward the equilibrium potential for Na^+ (E_{Na^+}), before the Na^+ channels rapidly inactivate. Parallel to the Na_v inactivation, the delayed voltage-activated K^+ (K_v) channels open, which gives rise to an outward K^+ current. The increase in the membrane permeability to K^+ repolarises the membrane toward the equilibrium potential for K^+ (E_{K^+}). After an action potential has occurred, there is a transient negative shift of the membrane potential, referred to as afterhyperpolarisation. The afterhyperpolarisation activates inwardly rectifying K^+ (K_{ir}) channels. The K_{ir}^+ channels reset the membrane potential to the resting value by allowing a flux of K^+ ions through the membrane. All of the different channels have specific activation and pharmacological properties, which allow their identification.

The Na_v channels, which are responsible for the rising phase of the action potential, are formed at the molecular level by the association of a set of pore-forming α and subsidiary β (β_1 , β_2 or β_3) subunits (Catterall et al., 2003; Hanck and Fozzard, 2007). The pore-forming α subunit is a product of a gene family with nine members from the Na_v1 gene family. The channels are denominated as $\text{Na}_v1.x$, where x is a number and denotes the specific channel

isoform and corresponds approximately to the order that each gene was identified. Accordingly, the channels are named $\text{Na}_v1.1-1.9$. The pore-forming subunits are formed by four large regions, each comprising six transmembrane (TM) domains and a P-loop between the fifth and the sixth TM helices. The association of the four P-loops form a pore through the membrane.

At the pharmacological level, the Na_v channels are characterised by their sensitivity to tetrodotoxin (TTX) and saxitoxin (STX). The channels are classified as either TTX sensitive or TTX resistant, depending on the TTX concentration that is necessary to inhibit the Na_v channels (Bosmans and Tytgat 2007; Koopmann et al., 2006; Lei et al., 2004; Narahashi, 2008). The TTX sensitive Na_v channels are inhibited by TTX concentrations of 10-100 nM, while the TTX resistant channels are blocked by TTX concentrations in the μM ranges (Lei et al., 2004). The TTX sensitivity is related to the presence of an aromatic amino acid residue (Y or F) at position 401 in the P-loop of the first large region (Fozzard and Lipkind, 2010; Lee and Ruben, 2008; Lipkind and Fozzard, 1994; Penzotti et al., 2001). Genetic and pharmacological studies have shown that $\text{Na}_v1.1-1.4$, 1.6, and 1.7 are TTX sensitive, while $\text{Na}_v1.5$, 1.8, and 1.9 are TTX resistant (Goldin, 2003; Koopmann et al., 2006; Lei et al., 2004; Narahashi, 2008).

The K_v channels are responsible for the repolarisation of the membrane. They are formed by association of four pore-forming α and four β auxiliary subunits. The pore-forming α subunits of the K_v channels have six transmembrane domains. They are produced by the K_v channel gene subfamily, which comprises four members, named *shaker*, *shab*, *shaw*, and *shal*, or K_v1 , K_v2 , K_v3 , and K_v4 , respectively. Each subfamily has characteristic activation and inactivation kinetic, as well as pharmacological sensitivity (Heitzmann and Warth, 2008; Nerbonne, 2000; Song, 2002). Despite contradictory observations, it is generally accepted that the members of the K_v1 channels have a fast activation, a slow inactivation and are sensitive to 4-aminopyridine (4-AP). The K_v3 channels activate very

quickly but inactivate slowly and are sensitive to tetraethylammonium (TEA). The K_v4 channels are fast activated and inactivated, and are sensitive to 4-AP. The K_v2 channels activate slowly and do not inactivate, and are inhibited by high TEA concentrations (Nerbonne, 2000). The fast activating channels, K_v1 , K_v3 , and K_v4 , are responsible for brief action potentials (Korn and Trapani, 2007) because they repolarise the membrane very quickly.

The K_{ir} channels belong to the family of two transmembrane domain (2 TM) K^+ channels with a pore forming region between the transmembrane domains (Heitzmann and Warth, 2008). Despite originating from 16 different genes, all K_{ir} channels share common properties. Each K_{ir} channel is formed by four α subunits assembled as homomer or heteromer. In all cases, the inward current increases with increasing external K^+ concentration ($[K^+]_o$), which indicates high specificity for K^+ . The most defining feature shared by all of the K_{ir} channels is the reversible blockage by externally applied Ba^{2+} (Olsen and Sontheimer, 2008). As the name implies, the K_{ir} channels preferentially conduct an inward current, although some subunits allow for outward currents. It is noteworthy that K_{ir} channels, while rectifying, are not voltage dependent. The apparent voltage sensitivity of these channels is related to a blockage of the channels by intracellular Mg^{2+} or polyamine ions, which are pushed into the channel pore by voltages above the E_{K^+} (Oliver et al., 2000; Panama and Lopatin, 2006; Ruppertsberg, 2000). This effect increases with membrane potentials that are more positive than E_{K^+} , resulting in a reduction of outward K^+ currents through the K_{ir} channels. While all K_{ir} channels rectify and pass K^+ ions into the cell more readily than they allow for K^+ efflux, the degree of rectification varies between the channel subtypes. The $K_{ir}1$, $K_{ir}4$, $K_{ir}5$, and $K_{ir}7$ subfamilies are weak inward rectifiers that permit considerable outward K^+ currents, while the $K_{ir}2$ and $K_{ir}3$ subfamilies rectify strongly, permitting little K^+ efflux (Bichet et al., 2003; de Boer et al., 2010; Hibino et al., 2010; Ruppertsberg, 2000). Moreover, the different K_{ir} channels

have specific pharmacology. The K_{ir1} and K_{ir4} channels are sensitive to pH. Internal acidification to pH values below 6.5 closes the channels (Dahlmann et al., 2004; Pearson et al., 1999). The K_{ir3} channels are activated by G protein-coupled receptors (Hibino et al., 2010). The K_{ir6} proteins form the K_{ATP} channels that are closed by internal ATP (Flagg et al., 2010; Hibino et al., 2010). A feature that is common to all vertebrate K_{ir} currents is a slow time-dependent inactivation, which increases with the hyperpolarisation and creates the negative bend in the current/voltage ($I(V)$) plot. While this could be interpreted as voltage-dependent gating, it actually reflects a voltage-dependent block of these channels by external Na^+ ions (Lee et al., 2007).

In this report, we show that primary osteoblasts and the osteoblast-like MG-63 cell line express sequentially activated Na_v , K_v and K_{ir} channels, which allow the cells to generate repetitive action potentials in response to a long lasting depolarisation. Herein, we discuss a potential role for the action potential in osteoblasts in processes such as differentiation, bone formation, and pathology.

Materials and Methods

Chemicals

If not otherwise stated, all chemicals and cell culture media were obtained from Sigma-Aldrich (Taufkirchen, Germany).

Cell culture

Primary human osteoblasts were cultured from bone chips obtained from patients undergoing total hip arthroplasty, following the protocol set by Gallagher (2003). The isolation protocol was approved by the local ethics committee of the Institute of Materials Research in Geesthacht, Germany. Briefly, cancellous bone was cut into 5-mm pieces. After removal of bone marrow, the bone chips were cultured in Dulbecco's modified eagle medium (DMEM) supplemented with 10% foetal bovine serum (PAA Laboratories GmbH, Linz, Austria), 100 U/ml penicillin, and 100 µg/ml streptomycin. The culture was maintained for approximately 10 days without medium change. Thereafter, the medium was changed every three days and cells were passaged after reaching 70-80% confluency.

The human osteosarcoma cell line, MG-63, was obtained from the European collection of cell cultures (ECACC, Salisbury, UK). They were cultured in DMEM supplemented with 10% foetal bovine serum, 100 U/ml penicillin, and 100 µg/ml streptomycin. The cultures were maintained at 37°C in a humidified atmosphere containing 5% CO₂ and 95% air. The culture medium was replaced every two to three days.

For patch-clamp experiments, cover slips (Ø 10 mm) were placed into dishes containing 4 ml of DMEM culture medium. The cells were seeded at a density of 1×10^5 cells/dish. The cells were used one to three days after seeding. For the primary cells, the cover slips were coated with collagen. The primary cells were cultured and used for up to five passages. For the MG-63 osteoblast-like cells, the cells were used up to passage 30.

For the RT-PCR experiments, the cells were cultured for two to five days and harvested when they were at least 80% confluent.

Functional identification of the expressed channels

The whole-cell patch-clamp technique was used to measure the different currents of the cells. All experiments were performed at room temperature. A cover slip with the cells was placed in a perfusion chamber containing 0.5 ml of a bath solution composed of (in mM): 145 NaCl, 5 KCl, 2 CaCl₂, 1 MgCl₂, 5 glucose, and 10 HEPES, (pH 7.4, 295 mosmol/l). The perfusion chamber was mounted onto an inverted microscope (Zeiss, Oberkochen, Germany). The cells were washed with 10 ml of bath solution at 1 ml/s. To visualise the cells, a CCD camera (Sony, Japan) and a video monitor was used. To navigate the patch-clamp capillaries onto the cells, a micromanipulator (Merzhäuser, Wetzlar-Steindorf, Germany) was used. The patch-clamp capillaries were filled with a pipette solution that contained (in mM): 145 K-gluconat, 5 KCl, 0.5 Na₂ATP, 2.5 MgATP, 0.5 CaCl₂, 1 EGTA, 1 glucose, and 10 HEPES (pH 7.4, 295 mosmol/l). To induce action potentials, depolarising currents were injected into the cells under a current-clamp modus with the patch-clamp amplifier EPC-7 (List Medical, Darmstadt, Germany) connected to a computer through an ITC-16 interface (Instrutech, Port Washington, USA). The currents were measured in voltage-clamp modus. From a constant holding voltage of -40 mV, test voltage pulses were applied from -150 mV to 90 mV for 1 s in 10 mV steps. The evoked currents were filtered at 3 kHz and sampled at 10 kHz. Pulse protocols, data acquisition, and analysis were performed using Pulse/PulseFit (HEKA, Lambrecht/Pfalz, Germany), Excel 2004 (Microsoft, Redmond, USA) and OriginPro 7.5 (Microcal Software, Inc., Northampton, USA).

Data analysis

The voltage-dependent channels were analysed between -150 mV and -60 mV with the amplitudes of the instantaneous current ($I_{(inst)}$) at the beginning of the voltage pulses measured and plotted against the corresponding voltage in an $I(V)$ plot. To describe the voltage dependence of the conductance of the channels, the macroscopic conductance (G) was calculated from the instantaneous current amplitudes, normalised to the maximal conductance (G_{max}). The corresponding values were plotted against the voltage in a $G(V)/G_{max}$ diagram. To estimate the activation parameters of the channels, the data points were fit with a simple Boltzmann distribution as given by the equation:

$G / G_{max} = 1 / (1 + e^{(U - U_{1/2}) \cdot \frac{zF}{RT}})$, where R , T , F have their usual meanings, $U_{1/2}$ represents the half-activation voltage at the point where 50% of the maximal conductance was reached, and z represents the number of apparent gating charges. Additionally, the steady state currents ($I_{(ss)}$) at the end of the voltage pulses were measured and plotted against the corresponding voltage in an $I_{ss}(V)$ plot. To account for the inactivation of the channels, the current-time relaxation between the instantaneous amplitude $I_{(inst)}$ and the steady state amplitude $I_{(ss)}$ was fit to the following single exponential function:

$I_{(t)} = (I_{(inst)} + I_{(ss)}) \cdot e^{-\frac{t}{\tau_i}} + I_{(ss)}$, where τ_i gives the voltage-dependent inactivation time.

Between -30 mV and 30 mV, the maximum amplitude of the voltage-activated inward current was measured and plotted against the corresponding voltage in an $I(V)$ plot. To describe the voltage dependence of the conductance of the channels, the macroscopic conductance (G) was calculated from the maximal amplitudes of the currents and plotted in a $G(V)/G_{max}$ diagram, and the activation parameters of the channels were obtained by fitting the data points with a simple Boltzmann distribution as described above.

Between -30 mV and 90 mV, the activated, delayed-activated outward currents were analysed in two steps. First, the amplitudes of the steady state currents ($I_{(ss)}$) at the end of the voltage pulse were measured and plotted against the corresponding voltage in an $I(V)$

plot. As described above, the macroscopic conductance (G) was calculated from the steady state current amplitudes, a $G(V)/G_{max}$ diagram was produced, and the data points were fit to a simple Boltzmann distribution to estimate the activation parameters of the channels. Second, the activation kinetics were estimated for each voltage pulse by fitting the time dependent increase of the current using the following simple exponential function: $I_{(t)} = (I_{(inst)} + I_{(ss)}) \cdot e^{-\frac{t}{\tau_a}} + I_{(ss)}$, where $I_{(inst)}$ and $I_{(ss)}$ are the instantaneous and the steady state current amplitudes, respectively, and τ_a gives the voltage dependent activation time.

Channel screening by RT-PCR

Total RNA from MG-63 cells (about 2 million cells) was extracted using the Qiagen RNeasy Mini Kit (Qiagen, Hilden, Germany). Genomic DNA was removed by digestion with RNase-free DNase (Fermentas, St. Leon-Rot, Germany) for 60 minutes at 37°C. First strand cDNA synthesis of the total RNA using the M-MLV reverse transcriptase (Invitrogen GmbH, Karlsruhe, Germany) was performed according to the manufacturer's protocol with a hexamer primer. cDNA fragments of the various K_{ir} , K_v , and Na_v channel subtypes were amplified using a set of designed sense and antisense primers (Primer-BLAST, <http://www.ncbi.nlm.nih.gov>), as shown in Table 1. PCR experiments were run on a 96 Universal Gradient PeqStar Thermocycler (PiqLab, Erlangen, Germany) in a final volume of 25 μ l containing 45 ng of first strand cDNA as the template. The amplification was performed in 44 cycles (15 sec at 94°C, 15 sec at $53 \pm 2^\circ\text{C}$, and 15 sec at 72°C). The PCR products were separated on 1.5% agarose gels and stained with GelRed (Biotium, Hayward, CA, USA).

Results

The firing of repetitive action potentials (Fig. 1) were induced in the primary isolated osteoblasts and in the osteoblast-like MG-63 cell line by injecting a depolarising current under the current-clamp modus of the whole-cell patch-clamp configuration. The action potentials were characterised by a long duration (60 ms), a high threshold (-20 mV), a non-complete repolarisation between the spikes, and a low frequency (a maximum of 5-6 Hz). The generation of repetitive action potentials in cells such as neurons or muscle cells is related to the concomitant expression and sequential activation of voltage-gated sodium (Na_v) and potassium (K_v) channels (Hodgkin and Huxley, 1952). Additionally, the inwardly rectifying potassium channels (K_{ir}) can participate in the generation of action potentials by controlling the resting membrane potential. Because we observed that the osteoblasts were able to generate action potentials, we analysed the voltage-dependent activation of the currents within the cells. In the primary osteoblasts, as well as in the MG-63 cells, we found a resting membrane potential of approximately -60 mV. To evaluate the ion channels expressed in the membranes of the cells, the cells were maintained at a holding potential of -40 mV and voltage pulses from -150 mV to 90 mV were applied for 1 s in 10 mV steps. Three distinct currents could be observed (Fig. 2): (i) an inward current activated by hyperpolarising voltages below -60 mV, (ii) an inward current activated by depolarising voltages between -30 mV and 30 mV, and (iii) a delayed-activated outward current evoked by depolarising voltages above -30 mV. Because these currents were observed in primary osteoblasts and in the osteoblast-like MG-63 cell line, the MG-63 cells were used for the further functional characterisation of the currents. In following, the electrical and pharmacological behaviour of these currents will be described.

The hyperpolarisation activated inward current

The hyperpolarisation-activated inward current was instantaneously activated between -60 mV and -150 mV in a voltage dependent manner. The instantaneous current was followed by a steady-state current (Fig 2a). The steady-state current increased with hyperpolarisation until -100 mV (Fig. 2B). At larger hyperpolarising voltages, an inactivation of the current was observed (Fig. 2A and B). The hyperpolarisation-activated inward current, which was observed at very low Cl⁻ concentrations in the internal solution, presented the following pharmacology: it was not significantly affected by the Cl⁻ channel inhibitor, 4,4'-diisothiocyano-2,2'-stilbene disulphonic acid (DIDS), it was inhibited by Ba²⁺ (Fig. 3A), and it was enhanced by an increased [K]_o. In addition, the increase in [K]_o suppressed the inactivation of the channel (Fig. 3B). The reverse potential of the current was estimated to be -70 mV and -10 mV at 5 mM and 55 mM of [K⁺]_o, respectively (Fig. 3B). To determine the voltage-dependent characteristics of the hyperpolarisation-dependent currents, we analysed the voltage-dependent activation of the instantaneous currents and the voltage-dependent kinetics of the current relaxation from the instantaneous current to the steady-state amplitudes. For the instantaneous current, macroscopic conductance-voltage ($G(V)$) curves were determined (Fig. 3C). The $G(V)/G_{max}$ diagrams show that the channels opened at hyperpolarising voltages. The half-maximal voltage of activation ($U_{1/2}$) of -73 mV and the apparent equivalent gating charge (z) of 2.3 were derived by fitting the $G(V)/G_{max}$ curve with a simple Boltzmann function (Fig. 3C). The kinetic of inactivation was voltage dependent. At -100 mV, the inactivation was very slow and the steady-state current could not be achieved during the duration of the pulse (1 s). The inactivation was very rapid at voltages below -120 mV and the steady-state current, representing 10% of the instantaneous current, was achieved within 400 ms (Fig. 2). The relaxation of the inactivated current could be fit by an exponential function, as described in the Materials and Methods (Fig. 3E insert). We found that the inactivation time decreased with

hyperpolarisation, from 330 ms at -100 mV to 163 ms at hyperpolarising voltages below -120 mV (Fig. 3D).

The depolarisation-activated inward current.

In 70% of the cells, depolarisation of the membrane to voltages above -30 mV induced an inward current (Fig. 1 A and Fig. 4) with the following characteristics: (i) the maximal amplitude of the current was achieved at 10 mV, (ii) the activation and the inactivation of the currents were very fast, and (iii) the current was abolished by depolarisations above 30 mV (Fig. 4A). In addition, the depolarisation-activated inward current showed a sensitivity to the internal Na^+ concentration ($[\text{Na}^+]_i$). At 10 mM internal Na^+ , the inward current was continuously reduced to achieve a complete run down within 5-10 min after establishment of the whole-cell configuration (results not shown). The run down was avoided at $[\text{Na}^+]_i$ of 1 mM. Additionally, the depolarisation-activated inward current was reversibly inhibited by 50 nM TTX (Fig. 4B).

To determine the voltage-dependent characteristics of the depolarisation-activated inward current, relative macroscopic conductance-voltage ($G(V)/G_{max}$) curves were determined (Fig. 4C). The $G(V)/G_{max}$ curves show that the currents were induced at voltages above -30 mV. The conductance increased with increasing depolarisation to achieve a maximum at a depolarisation between 0 and 10 mV. The half-maximal activation voltage ($U_{1/2}$) of -9 mV and the equivalent gating charge (z) of 4.2 were derived by fitting the $G(V)/G_{max}$ curve with a simple Boltzmann distribution.

The depolarisation-activated outward current

The delayed-activated outward current was observed in all cells when depolarising voltages above -30 mV were applied. The current showed a slow activation followed by a steady-state current, $I_{(ss)}$, which increased with increasing voltages (Fig. 2). The

depolarisation-activated outward current presented the following pharmacology: (i) the Cl⁻ channel inhibitor DIDS reduced the current by 20-30%, and (ii) TEA, the inhibitor of the voltage-dependent K⁺ channels, reduced the current by 70-80% (Fig. 5A). To determine the voltage-dependent characteristics of the hyperpolarisation-dependent currents, we analysed the voltage-dependent activation of the steady-state current and the kinetics of voltage-dependent activation of the current. The relative steady-state macroscopic conductance-voltage ($G(V)/G_{max}$) curves were determined (Fig. 5B). The $G(V)/G_{max}$ diagrams show that the channels opened at depolarizing voltages above -30 mV. The conductance increased with the voltage to achieve a maximum at 20 mV. The half-maximal voltage of activation ($U_{1/2}$) of -8 mV and the equivalent gating charge (z) of 4.8 were derived by fitting the $G(V)/G_{max}$ curves with a simple Boltzmann distribution.

The activation kinetic was characterised by fitting the currents during the activation time with the single exponential function (Fig. 5C insert) described previously. At very low voltages (-30 mV to 0 mV), the activation was very slow and could not be fit by the exponential equation. This was not due to the depolarisation-activated inward current described above because the inhibition of the current with TTX did not affect the activation kinetics of the channels (Fig. 5C). Considering the voltage dependency of the activation, we found that the activation time (τ_a) decreased with the depolarisation. A maximal value of 90 ms for τ_a was estimated at 0 mV, and it decreased to reach a minimal value of 13 ms at 50 mV (Fig. 5C).

Discussion

We were able to show, for the first time, that osteoblasts are able to generate repetitive action potentials (Fig. 1). Action potentials in neurons and muscle cells have been correlated with the sequential opening of voltage-gated Na^+ and K^+ channels (Hodgkin and Huxley, 1945; 1952). In primary osteoblasts and in the osteoblast-like MG-63 cells, we discovered a membrane potential of approximately -60 mV. The region between -60 mV and -40 mV was characterised by non-activation of specific currents flanked by two distinguishable regions where voltage pulses activated different currents (Fig. 2). On the left side, the voltage pulses (-150 mV to -60 mV) activated an inward current. On the right side, the voltage pulses between -30 mV and 30 evoked a rapid activated and inactivated inward current and the pulses from -30 mV to 90 mV induced a delayed-activated current (Fig. 2).

The hyperpolarisation-activated inward currents

The hyperpolarisation between -150 mV and -60 mV induced an inward current characterised by voltage-dependent inactivation (Fig. 2, Fig. 3A). The inactivation could be suppressed by reducing the external Na^+ concentration (results not shown). Inward currents, induced by hyperpolarisation of the cell, are due to an influx of cations (K^+) or to an efflux of anions (Cl^-). The observed inward current was registered in the absence of the internal Cl^- , was not affected by DIDS and was completely abolished by an external application of Ba^{2+} (Fig. 3A). Moreover these channels were inactivated by external Na^+ (Data not shown), a characteristic feature of K_{ir} channels (Lee et al., 2007). Additionally, the density of the current increased with increasing $[\text{K}^+]_0$, and its reversal potential followed the E_{K^+} from -70 mV to -10 mV at $[\text{K}^+]_0$ of 5 mM and 55 mM, respectively (Fig. 3B). These properties indicate that the hyperpolarisation-activated inward current was due to the opening of the K_{ir} channels. The current could be measured at an internal pH of 6.5,

indicating that it was not related to the pH sensitive channel K_{ir1} or the K_{ir4} subfamily (Dahlmann et al., 2004; Pearson et al., 1999). The current was measured without the activation of G protein-coupled receptors, which suggests that the current does not rely on the G protein-activated K_{ir3} channels (Flagg et al., 2010; Hibino et al., 2010). Finally, the current was measured in the presence of internal ATP, which shows that the ATP-sensitive K_{ir6} channels (Hibino et al., 2010) were not involved. The hyperpolarisation-activated inward current was observed at voltages below -60 mV (Fig. 2 and Fig. 3), indicating a strong rectification. These results suggest that the current was related to the channels of the K_{ir2} subfamily (Hibino et al., 2010). This conclusion was confirmed by RT-PCR experiments, which show clear mRNA expression of the $K_{ir2.1}$, $K_{ir2.3}$, and $K_{ir2.4}$ channels, the prototypes of the strongly rectifying K_{ir} channels (Fig. 6).

We found that the current was characterised by a half-activation voltage of -73 mV and an apparent gating charge of 2.3. As for the apparent gating charge, it has been shown that in cultivated cells, the inward K^+ channels have a z value between four and six (Hille, 2003). Experiments in expression systems, such as *Xenopus* oocytes, estimate the z value of the K_{ir} channels to 11-17. These values correspond to the charges of the S4 domain of the channel subunits. The fact that they are not found in the cultivated cells was interpreted as an indication of a reduced population of the channels in the membrane (Hille, 2003). This interpretation can be applied to our experiments. We can assume that the MG-63 cells, as well as the primary osteoblasts, express a low density of the $K_{ir2.x}$ channel family. This conclusion is supported by the reduced current density measured, with a maximum of -31 pA/pF (Fig. 2B and Fig. 3A).

The depolarisation-activated inward current

Depolarisation of the cells between -30 mV and 30 mV correlated with a rapid activation followed by an inactivation (Fig. 1 and Fig. 4). These are properties of Na_v channels as

they have been defined by Hodgkin and Huxley (1952). The measured currents were characterised by a half-activation voltage of -8 mV and by an apparent gating charge of 4.8. These parameters were also found for the Na⁺ channels in the giant axon of the crayfish (Hodgkin and Huxley, 1952). Therefore, we assume that the depolarisation-activated inward current was related to activation of Na_v channels (Fig. 4C). New data from *Xenopus* oocytes show a *z* value of 11-16 for the Na_v channels (Hille, 2003). As with the K_{ir} channels, the discrepancy between the values obtained from the original cells and from expression systems has been interpreted as an indication of a reduced channel density in the original cells in comparison to the expression systems (Hille, 2003). Therefore, we assume that we have a reduced density of the Na_v channels, which correlated with the observed, reduced maximal current density of -9 pA/pF (Fig. 4A). The conclusion that depolarisation opened the Na_v channels is supported by the observation that an increase in internal [Na⁺], or by an increase in the external Ca²⁺ concentration, inhibited the current (results not shown). The current was completely suppressed by the application of 50 nM TTX (Fig. 4B), which indicates that the cells are expressing TTX sensitive channels. The pore forming α subunits of the Na_v channels are produced by a gene family with the nine members, named Na_v1.1-1.9, which evolved from a single gene by gene duplication (Goldin, 2002). The genetic differences correlate to differences in the sensitivity of the channels to TTX. The channels, Na_v1.1-1.4, 1.6 and 1.7, are classified as TTX sensitive because they are inhibited by low concentrations of TTX (10-100 nM), while the TTX resistant channels (Na_v1.5, 1.8 and 1.9) are inhibited by higher TTX concentrations (10-100 μ M) (Goldin, 2003; Koopmann et al., 2006; Lei et al., 2004; Narahashi, 2008). In our experiments, we found that the depolarisation-activated inward current was suppressed by 50 nM TTX (Fig. 4B). We hypothesized that the osteoblasts expressed the TTX sensitive channels, Na_v1.1-1.4, 1.6, and 1.7. This hypothesis was verified by RT-PCR experiments, which showed an expression of the TTX sensitive Na_v1.3, 1.4, 1.6, and 1.7 channels both

in the primary osteoblasts and in the MG-63 osteoblast-like cells (Fig. 6A, B, and C). Additionally, we found mRNA of the TTX-resistant $\text{Na}_v1.5$ channel (Fig. 6). However, because we observed that the Na^+ current was completely abolished at very low TTX concentrations, we predict that the mRNA of $\text{Na}_v1.5$ is not translated into functional channels. Further, we were not able to determine whether $\text{Na}_v1.3$, 1.4, 1.6, and 1.7 equally participate in the formation of the observed channels. Biochemical and cell imaging experiments, beyond the present scope of this paper, should clarify this issue.

The delayed, depolarisation-activated outward current

Depolarisation above -30 mV gave rise to a delayed-activated outward current, which increased with the increasing depolarisation (Fig. 2 and Fig. 5A). The Cl^- channel inhibitor, DIDS, reduced the currents by 20-30% and the K^+ channel inhibitor suppressed 70-80% of the current (Fig. 5). These results indicate that the major portion of the outward current was related to the opening of the voltage-activated K^+ channels (K_v). The activation parameters of this current, given by the Boltzmann fitting, had a half-activation of 8 mV and an apparent gating charge of 4.2 (Fig. 5B). The half-activation and the gating charge values indicate that there was a reduced population of K_v channels (Hille, 2003). The channels displayed a slow activation, however, an inactivation was not observed (Fig. 2A and Fig. 5C insert). At the pharmacological level, the channels were inhibited by TEA (Fig. 5A) and were insensitive to Ba^{2+} and 4-AP (results not shown). The voltage-activated outward K^+ channels are responsible for the membrane repolarisation after an action potential. They belong to the family of the six TM K_v channels. This family is divided into four subfamilies, K_v1-4 . Each subfamily is characterised by unique activation and inactivation kinetic as well as by a specific pharmacology (Heitzmann and Warth, 2008; Nerbonne, 2000; Song, 2002). The members of the K_v1 and K_v4 subfamilies are characterised by fast activation, a fast inactivation mechanism, and are sensitive to 4-AP.

The K_v3 channels activate very fast, have a slow inactivation, and are sensitive to TEA. The K_v2 channels have a slow activation mechanism, are sensitive to TEA, and do not inactivate (Nerbonne, 2000). Taken together, this implies that the primary cells, as well as the MG-63 cells, express channels of the K_v2 subfamily. This conclusion was reached because the channels observed displayed slow activation and did not inactivate, and were inhibited by TEA. This assumption is also supported by the voltage-dependent activation kinetic of the channels. We show that the channels have a voltage-dependent activation time (τ_a) with a minimal value of 10 ms, which was achieved at 40 mV (Fig. 5C). A comparable activation time was observed for the K_v2.1 channels expressed in *Xenopus* oocytes (Consiglio and Korn, 2004). Furthermore, the RT-PCR analysis confirmed the expression of K_v2.1 (Fig. 6).

Cellular consequences of the expression of the voltage-activated channels

The concomitant presence of Na_v, K_v, and K_{ir} channels in the neurons, as well as their sequential activation during the depolarisation and repolarisation process, was postulated as the basis of the action potential (Hodgkin and Huxley, 1952). In this report, we observed that MG-63 cells and primary osteoblasts expressed K_{ir}, Na_v and K_v channels, which were sequentially activated upon depolarisation. In addition, the cells were able to generate action potentials (Fig. 1). The pharmacology and the electrophysiological parameters of the channels suggests that different types of K_{ir}, Na_v and K_v channels are present, however at a low density compared to excitable cells, such as neurons. We observed that the cells exclusively expressed the slowly activated K_v2 channel subtype. The low channel density and the slow activation of K_v channels are likely responsible for the long duration of the action potential. In the same way, the low density of the Na_v channels could explain the low maximal frequency of the action potential (5 Hz) observed in the cells (Fig. 1). The K_{ir} channels are responsible for setting the resting membrane potential and controlling the

excitation threshold. In osteoblasts, we observed the expression of the strongly rectifying $K_{ir2.1}$, $K_{ir2.3}$, and $K_{ir2.4}$ channels. This finding correlates with the polarisation (-60 mV). Moreover the strongly rectifying K_{ir} channels and the low density of slow activating K_v channels could explain the non-complete repolarisation observed (Fig. 1).

The significance of the action potentials in the osteoblasts is not clear. In excitable cells, the firing of action potentials is a marker of differentiation. We can assume that the presented action potentials and the expressed ion channels in the MG-63 osteoblasts and in the isolated primary osteoblasts could be a characteristic of a developmental state of osteoblast during osteogenesis, which has not been described so far. Moreover, osteoblasts isolated from different persons are variable with respect to the capacity to generate action potentials (result not shown). This may be related to the developmental and pathological state of the isolated cells, for example, whether cells were isolated from healthy or pathogenic (mainly osteoporotic) tissues. Alterations during pathological or developmental changes in bone tissue are mainly analysed on the genetic level (signalling pathways), and the hormonal regulation of the ion channels has not been of great interest as of yet (Zaidi, 2004). Evidence has accumulated that ion channels such as melastatin like transient receptor potential 7 (TRPM7), chloride channels, or voltage-operated calcium channels (VOCCs) are involved in development, proliferation and differentiation of osteoblasts (Abed and Moreau, 2009; Wang et al 2010; Zahanich et al, 2005). The present report shows for the first time action potentials and characterises the expressed voltage dependent channels responsible for the generation the action potentials in the osteoblasts. This report represents therefore a further attempt to characterise the functional physiology of developing osteoblasts.

Acknowledgments

The authors thank Prof. Dr. Helge Küster and his team for discussion on the manuscript.

The work was supported by the BMBF project NANOTOME (Biophotonik III), the DFG project (Transregio 37) and by Boehringer Ingelheim International GmbH.

References

- Abed E. and Moreau R. (2009) Importance of melastatin-like transient receptor potential 7 and magnesium in the stimulation of osteoblast proliferation and migration by platelet-derived growth factor *Am. J. Physiol. Cell Physiol.* **297**, C360-C368.
- Bezanilla, F. (2007) Voltage-gated ion channels. In Chung S.H., Andersen O.S. Krishnamurthy, V. (Ed.) Biological membrane ion channels: dynamics, structure and applications. Springer Science + Business Media, LLC. PP: 81-118
- Bichet, D., Haass, F.A., and Jan, L.Y. (2003) Merging functional studies with structures of inward-rectifier K⁺ channels. *Nat. Rev. Neurosci.* **4**, 957-967
- de Boer, T.P., Houtman, M.J.C., Compier, M., and van der Heyden, M.A.G. (2010) The mammalian K_{ir}2.x inward rectifier ion channel family: expression pattern and pathophysiology. *Acta Physiol.* **199**, 243-255
- Bosmans, F. and Tytgat, J. (2007) Voltage-gated sodium channel modulation by scorpion α -toxins. *Toxicon* **49**, 142-158
- Catterall, W.A., Goldin, A.L., and Waxman, S.G. (2003). International union of pharmacology. XXXIX. Compendium of voltage-gated ion channels: sodium channels. *Physiol. Rev.* **55**, 575-578
- Clay, J.R. (2005) Axonal excitability revisited. *Prog. Biophys. Mol. Biol.* **88**, 59-90
- Consiglio, J.F. and Korn, S.J. (2004) Influence of permeant ions on voltage sensor function in K_v2.1 potassium channel. *J. Gen. Physiol.* **123**, 387-400
- Dahlmann, A., Li M., Gao, Z.H., McGarrigle, D., Sackin, H., and Palmer, L.G. (2004) Regulation of K_{ir} channels by intracellular pH and extracellular K⁺: mechanism of coupling, *J. Gen. Physiol.* **123**, 441-454

Flagg, T.P., Enkvetchakul, D., Koster, J.C., and Nichols, C.G. (2010) Muscle K_{ATP} channels: recent insights to energy sensing and myoprotection. *Physiol. Rev.* **90**, 799-829

Fozzard, H.A. and Lipkind, G.M. (2010) The tetrodotoxin binding site is within the outer vestibule of the sodium channel. *Mar. Drugs* **8**, 219-234

Gallagher J.A. (2003) Human osteoblast culture. *Methods Mol. Med.* **80**, 3-18

Goldin, A.L. (2002) Evolution of voltage-gated Na^+ channels. *J. Exper. Biol.* **205**, 575-584

Hanck, D.A. and Fozzard, H.A. (2007) Voltage-gated sodium channels. in Chung S.H., Andersen O.S., and Krishnamurthy V. (Eds) Biological membrane ion channels: dynamics, structure and applications. Springer Science + Business Media, LLC. PP: 219-239

Heitzmann, D. and Warth, R. (2008) Physiology and pathophysiology of potassium channels in gastrointestinal epithelia. *Physiol. Rev.* **88**, 1119-1182

Hibino, H., Inanobe, A., Furutani, K., Murakami, S., Findlay, I., and Kurachi, Y. (2010) Inwardly rectifying potassium channels: their structure, function, and physiological roles. *Physiol. Rev.* **90**, 291-366

Hille, B. (2003) Ion channels of excitable membranes, 3rd edn. Sinauer Associates Press, Sanderland

Hodgkin, A.L. and Huxley, A.F. (1945) Resting and action potentials in single nerve fibres. *J. Physiol.* **104**, 176-195

Hodgkin, A.L. and Huxley, A.F. (1952) A quantitative description of membrane current and its application to induction and excitation in nerve. *J. Physiol.* **117**, 500-544.

Koopmann, T.T., Bezzina, C.R., and Wilde, A.A.M. (2006) Voltage-gated sodium channels: action players with many faces. *Ann. Med.* **38**, 472-482

Korn, S.J. and Trapani, J.G. (2007) Voltage-gated potassium channels. In Chung S.H., Andersen O.S. Krishnamurthy V. (Ed.) Biological membrane ion channels: dynamics, structure and applications. Springer Science + Business Media, LLC. PP: 119-170

- Lee, C.H. and Ruben, P.C. (2008) Interaction between voltage-gated sodium channels and the neurotoxin, tetrodotoxin. *Channels* **2**, 407-412
- Lee, D.H., Kimm, K., Kim, H.L, and Han, B.G. (2007) Heterogeneous composition of voltage-dependent K⁺ currents in hepatic stellate cells. *Yonsei Med. J.* **48**, 684-693
- Lei, M., Jones, S.A, Liu, J., Lancaster, M.K., Fung, S.S.M., Dobrzynski, H., Camelliti, P., Maier, S.K.G., Noble, D., and Boyett, M.R. (2004) Requirement of neuronal- and cardiac-type sodium channels for murine sinoatrial node pacemaking. *J. Physiol.* **559**, 835-848
- Lipkind, G.M. and Fozzard, H.A. (1994) A structural model of the tetrodotoxin and saxitoxin binding site of the Na⁺ channel. *Biophys. J.* **66**, 1-13
- Narahashi, T. (2008) Tetrodotoxin: a brief history. *Proc. Jpn. Acad., Ser. B. Phys. Biol.Sci.* **84**, 147-154
- Nerbonne, J.M. (2000) Molecular basis of functional voltage-gated K⁺ channel diversity in the mammalian myocardium. *J. Physiol.* **525**, 285-298
- Oliver, D., Baukrowitz, T., and Fakler, B. (2000) Polyamines as gating of inward rectifier K⁺ channels. *Eur. J. Biochem.* **267**, 5824-5829
- Olsen, M.L. and Sontheimer, H. (2008) Functional implications for Kir4.1 channels in glial biology: from K⁺ buffering to cell differentiation. *J. Neurochem.* **107**, 589–601
- Panama, B.K. and Lopatin, A.N. (2006) Differential polyamine sensitivity in inwardly rectifying Kir2 potassium channels. *J. Physiol.* **571**, 287-302
- Penzotti, J.L., Lipkind G., Fozzard, H.A., and Dudley, Jr. S.C. (2001) Specific neosaxitoxin interactions with the Na⁺ channel outer vestibule determined by mutant cycle analysis. *Biophys. J.* **80**, 698-706
- Pearson, W.L., Dourado, M., Schreiber, M., Salkof, L., and Nichols, C.G (1999) Expression of a functional Kir4 family inward rectifier K⁺ channel from a gene cloned from mouse liver. *J. Physiol.* **514**, 639-653

- Ruppersberg, J.P. (2000) Intracellular regulation of inward rectifier K⁺ channels. *Pflügers arch. - Eur. J. Physiol.* **441**, 1-11
- Song, W.J. (2002) Genes responsible for native depolarization-activated K⁺ currents. *Neurosci. Res.* **42**, 7-14
- Wang, H., Mao, Y., Zhang, B., Wang, T., Li, F., Fu, S., Xue, Y., Yang, T., Wen, X., Ding, Y., and Duan, X. (2010) Chloride channel ClC-3 promotion of osteogenic differentiation through Runx2. *J. Cell Biochem.* **111**, 49-58.
- Zahanich, I., Graf E.M., Heubach, J.F., Hempel, U., Boxberger, S., and Ravens, U. (2005) Molecular and functional expression of voltage-operated calcium channels during osteogenic differentiation of human mesenchymal stem cells. *J. Bone Miner. Res.* **20**, 1637-1646
- Zaidi, M. (2007) Skeletal remodeling in health and disease. *Nat Med* **13**, (7), 791-801

Table and Figure Legends

Table 1

List of the primers used for the RT-PCR.

Figure 1

Depolarisation induced action potentials. The injection of currents between 50 and 100 pA generates action potentials in the cells. The frequency increased with the intensity of the depolarising current to a maximum of six spikes during the depolarisation period (1 s).

Figure 2

The current elicited by different voltage pulses. (A) Original traces of the currents evoked by voltage pulses as indicated. Hyperpolarising voltages between -150 mV and -60 mV induced inward currents. (B) The I(V) diagram of the observed currents. The current voltage relationship (I(V)) of the instantaneous current amplitude and the steady state current amplitude were measured in the first and in the last 10 ms of the voltage pulses. The results are given as an average, and the error bars represent the SEM for eight experiments. In addition, similar currents could be measured in the cultivated primary osteoblasts.

Figure 3

Pharmacological and electrical characterisations of the hyperpolarisation-activated currents.

(A) A voltage/current density plot is shown. With respect to the control conditions, the diagram shows that the current was significantly reduced by DIDS and was completely inhibited by Ba^{2+} . The results are averages of 20 (control), nine (Ba^{2+}) and eight (DIDS) cells, the error bars represent the SEM. (B) The current density was potentiated by $[\text{K}^+]_o$ increase. The results of each curve are an average of five cells, and the error bars represent the SEM. (C) The voltage-dependent membrane conductance $G(V)/G_{max}$. The solid line represents a fit of the data points with a simple Boltzmann distribution. This allowed us to estimate a half-activation voltage of -73 mV and an apparent gating charge of 2.3. Each point represents an independent experiment ($n = 10$). (D) The voltage-inactivation kinetics of the hyperpolarisation induced currents. The current relaxation observed at each voltage pulse was fitted with a simple exponential function (insert). The voltage-dependent inactivation time, τ_i , decreased with increasing hyperpolarisation. From a maximal value of 330 ms at -100 mV, τ_i reached the minimal value of 164 ms for voltages below -120 mV. The results are given as an average, and the error bars represent the SEM for 29 cells

Figure 4

The depolarisation-activated inward current. (A) The diagram shows the maximal current density evoked by the different voltage pulses. These currents were observed in 73% of the cells (16 out of 22). The resulting curve is an average of 16 cells, the error bars represent the SEM. (B) The current could be suppressed by 50 nM TTX. The TTX inhibition was reversible (not shown). (C) The voltage-dependent membrane conductance $G(V)/G_{max}$. The solid line represents a fit of the data points with a simple Boltzmann function. A half-activation voltage, $U_{1/2}$, of -8 mV and an apparent gating charge, z , of 4.2 were estimated ($n = 9$).

Figure 5

The pharmacological and electrical properties of the delayed outward current. (A) The currents were activated at depolarisation voltages above -30 mV. TEA reduced the current amplitude by more than 70%. DIDS reduced the current by 20-30% (result not shown). The results are averages of 20 cells and eight cells, respectively, for the control experiments and the blockage with TEA. The error bars represent the SEM. (B) The normalized voltage-dependent conductance $G(V)/G_{max}$. The solid line represents a fit of the data points with a simple Boltzmann function. This allowed an estimation of the half-activation voltage, $U_{1/2}$, of -8 mV and an apparent gating charge, z , of 4.8. The results are an average of 11 cells. (C) The activation kinetics of the current was estimated by fitting the time course of the voltage-activated currents (insert) with a single exponential function. The activation time, τ_a , decreased with increasing voltage from a maximal value of 90 ms at 0 mV and reached a minimal value of 13 ms at 50 mV. The results are given as an average and the error bars represent the SEM for 29 cells

Figure 6

The channels expressed in the cells as determined by RT-PCR.

Tables and Figures

Table 1

Gene name	Accession No.	Forward primer (5' -> 3')	Reverse primer (5' -> 3')	Product size (bp)
Nav1.1	NM_001165963	TGTTTCACTGAAGGCTGTGTACAA	GCCAACACCAGGCATTGGTG	322
Nav1.2	NM_021007	TCACGAAATGTAGAATTACAACCCA	TCAAAGACTTGTTTGGTTACAAAATCA	302
Nav1.3	NM_006922	TTCAGTGCATTGTGATGGCA	TTGGTTTCAAAGCAGAATCGC	287
Nav1.4	NM_000334	GGAGTCACTGGCAGCCATAG	CATGCTGAACAGCGCATGGA	340
Nav1.5	NM_198056	CAAGTGAATTCGAGGAGATGCT	CCGATGATCTTGATGAGTGTGT	274
Nav1.6	NM_014191	CTAGGCAAGTCTTGGTGGATC	CAGCCACAATGAGGAAGTCC	283
Nav1.7	NM_002977	GGGTGTCGGCTTTCCAATT	GGCAACATTGCCATCTTTTCA	276
Nav1.8	NM_006514	TCCCATTGGATCCCTCGAA	AAATAAACTGAACCACGAGTGGA	398
Nav1.9	NM_014139	GCAGGCTGTTTTATTCCC	ACATGCTGAACAATGAATGGACTG	472
Kir2.1	NM_000891	TCGCTTTTTACAAACCACTGGA	TTCTGCTTTGGAAAACAGTCTGA	277
Kir2.2	NM_021012	ATCCGCTTTCAGAGAAGAC	GCGGCTCCTCTTGAGTTC	300
Kir2.3	NM_152868	GGTGGGGGTTTCAAAGACTG	ACAGTCATGCAAAAGAAACGC	286
Kir2.4	NM_013348	GCTGGTCTTCAGCGAGAAC	TAGTCATACAGAGGACTGGC	271
Kv2.1	NM_004975	ACCTACTGGAGAAGCCCAATT	TAGTATGGCAGAATGGCCAAC	292
Kv2.2	NM_004770	ATGAACGAAGAAGCTGAGGCG	TGCTAATTGGCGGTTGTCATT	261
Kv3.1	NM_004976	GAGATGACCAAGCGCCTG	ATGTAGGTAAGGAAGGCTCC	296
Kv3.2	NM_139136	ATCCGCAGATCACAGAATGAAG	GTTCTCGATCTTGCCCATCTC	272

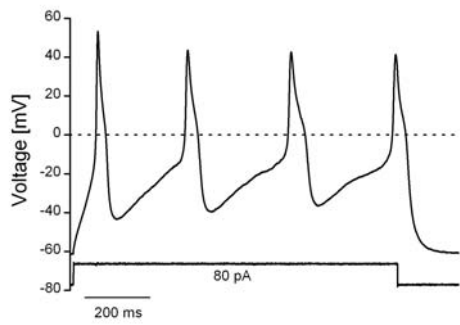


Figure 1

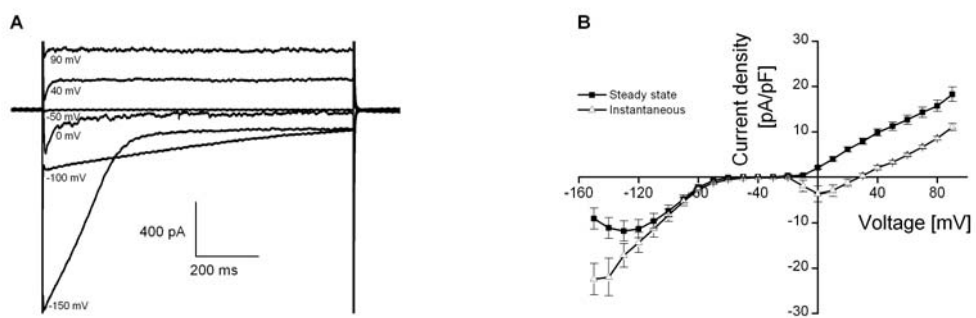


Figure 2

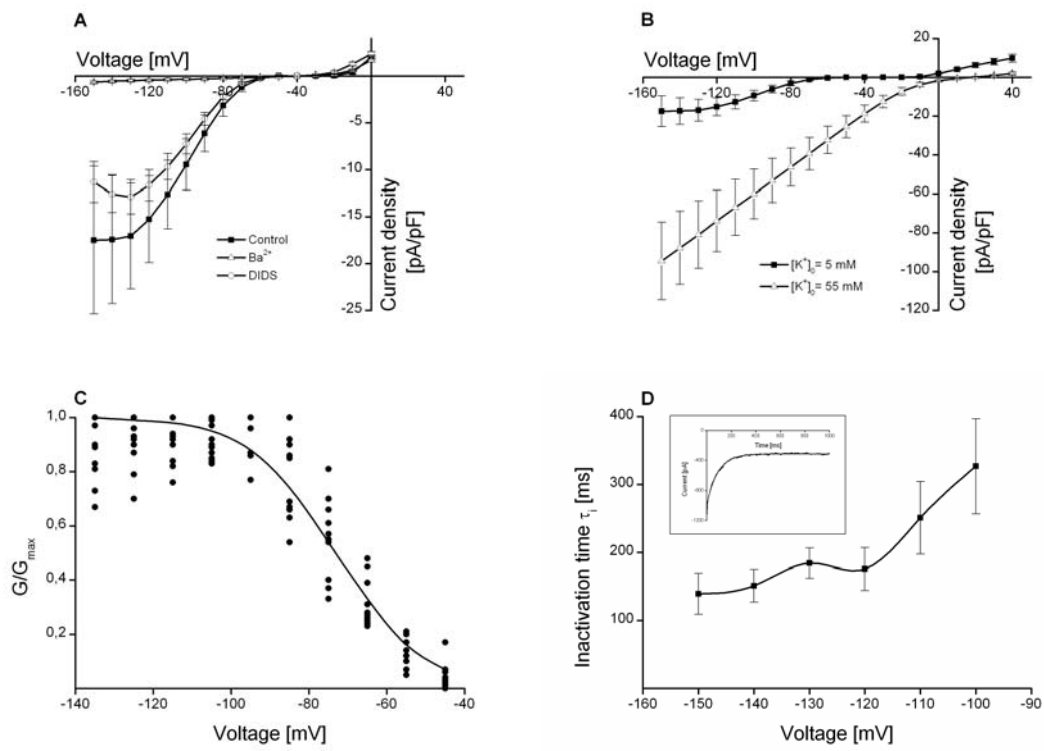


Figure 3

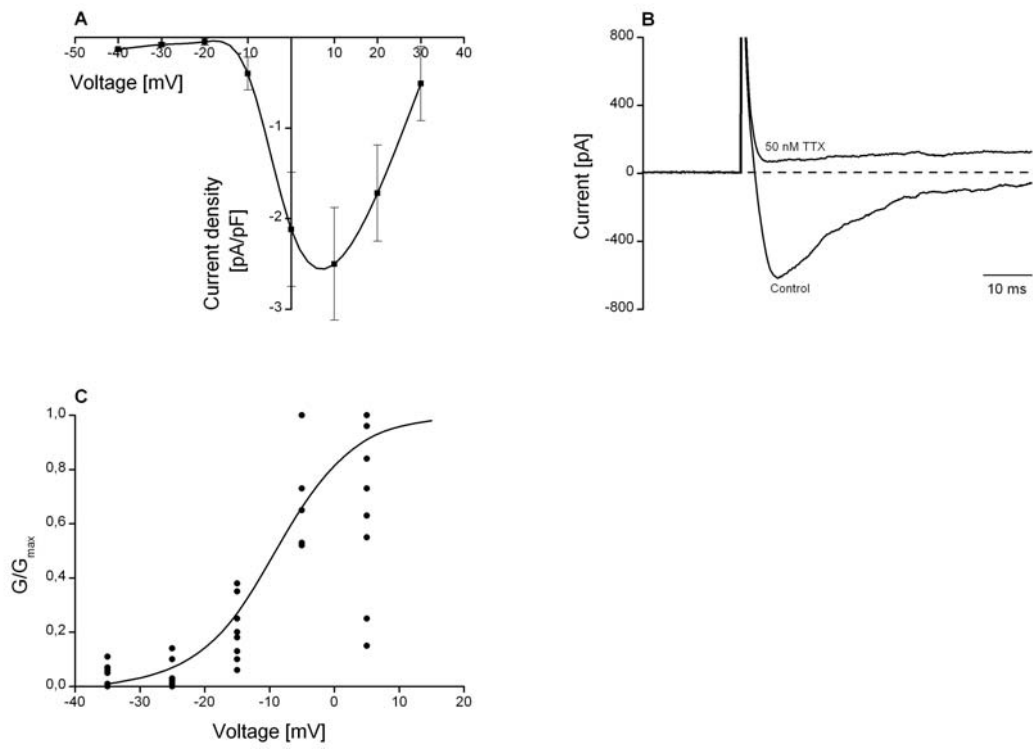


Figure 4

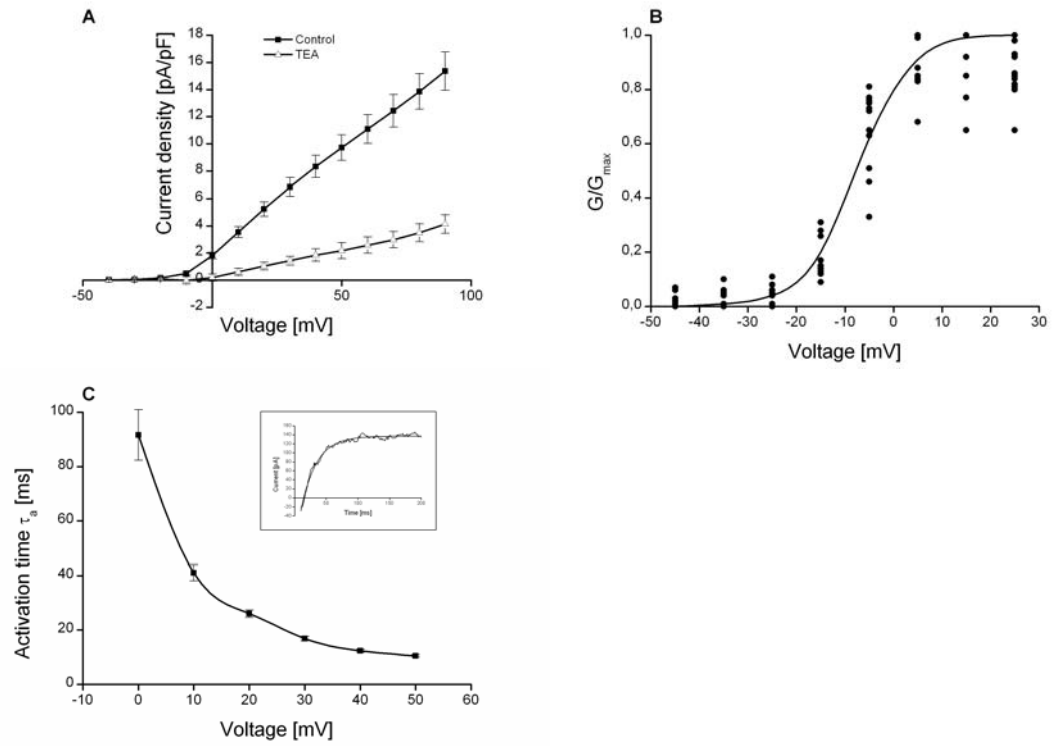


Figure 5

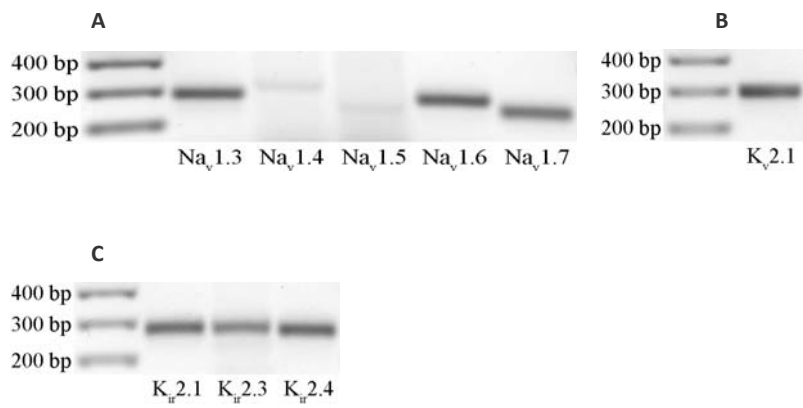


Figure 6